Biol. Cybern. 53, 93–108 (1985)

Biological Cybernetics

An Improved Neural-Network Model for the Neural Integrator of the Oculomotor System: More Realistic Neuron Behavior

Stephen C. Cannon* and David A. Robinson

Departments of Biomedical Engineering and Ophthalmology, The Johns Hopkins University, Baltimore, MD 21205, USA

Abstract. The discharge rates of premotor, brain-stem neurons that create eye movements modulate in relation to eye velocity yet firing rates of extraocular motoneurons contain both eye-position and eye-velocity signals. The eye-position signal is derived from the eye-velocity command by means of a neural network which functions as a temporal integrator. We have previously proposed a network of lateral-inhibitory neurons that is capable of performing the required integration. That analysis centered on the temporal aspects of the signal processing for a limited class of idealized inputs. All of its cells were identical and carried only the integrated signal. Recordings in the brain stem, however, show that neurons in the region of the neural integrator have a variety of background firing rates, all carry some eye-velocity signal as well as the eye-position signal, and carry the former with different strengths depending on the type of eye movement being made. It was necessary to see if the proposed model could be modified to make its neurons more realistic.

By modifying the spatial distribution of afferents to the network, we demonstrate that the same basic model functions properly in spite of afferents with nonuniform background firing rates. To introduce the eye-velocity signal a double-layer network, consisting of inhibitory and excitatory cells, was necessary. By presenting the velocity input to only local regions of this network it was shown that all cells in the network still carried the integrated signal and that its cells could carry different eye-velocity signals for different types of eye movements. Thus, this model stimulates quantitatively and qualitatively, the behavior of neurons seen in the region of the neural integrator.

* Address for correspondence

1 Introduction

The eye-movement control system contains a neural network that integrates with respect to time. Commands for various types of conjugate eye movements (both eyes moving together) appear in the brain stem as neurally-encoded, eye-velocity commands. The motoneurons, however, require an eye-position command as well (for a review see Robinson 1981) and a neural integrator must exist to convert the velocity to the position command. Theoretical arguments (Robinson 1975) support the idea that all velocity commands for saccadic, vestibular, optokinetic, and pursuit eye movements share a single, final common integrator and recent lesion experiments confirm it (Cannon and Robinson 1985; Cheron et al. 1985). These experiments also place this integrator, for horizontal eye movements, in the region of the rostral medial vestibular nucleus and nucleus prepositus hypoglossi.

The question arises of how to build an integrator with neurons. Positive feedback has always been the favored hypothesis. If cells could excite themselves through local network connections, then activity, once started, would be perseverated: integration. There were two problems with this proposal. The first was that all the neurons concerned had a high, background discharge rate, of about 100 spikes/s, upon which rode the signal to be integrated. How could one integrate the signal without the background? The second was that in order to build the oculomotor integrator with a leak rate corresponding to a time constant of 20 s (Becker and Klein 1973) out of neurons with a membrane time constant of 0.005 s, an increase of four orders of magnitude is required. This demands great accuracy in the amount of positive feedback required and such a system may not be robust – it may be unreasonably sensitive to small fluctuations in its parameters.

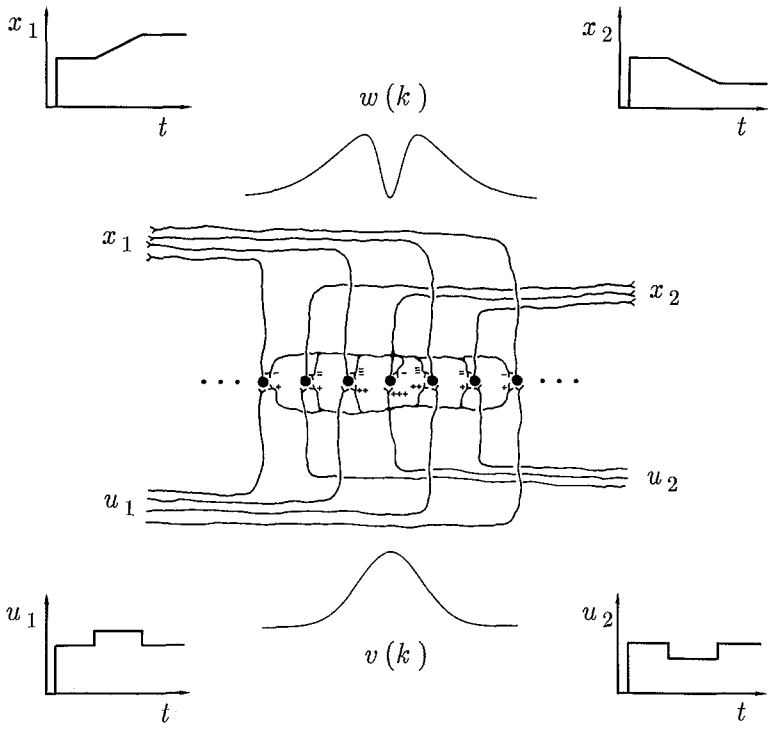

Fig. 1. Schematic representation of a lateral-inhibitory network. The lateral-inhibitory connections and afferent arborizations are illustrated for only the central neuron for reasons of clarity. The smooth curves above, $w(k)$, and below, $v(k)$, the network depict the synaptic weighting of the inhibitory and afferent profiles, respectively. The insets represent the input (u_1 and u_2) and output (x_1 and x_2) firing rates for a hypothetical step increase in background firing rate, followed by a brief, rectangular pulse input, modulated in push–pull. The background firing rate is not integrated, whereas the push–pull component or motor command is. Notice the high degree of mixing or interdigitation of the afferents originating from the push versus the pull gaze centers

Cannon et al. (1983) proposed a neural network utilizing lateral inhibition (Fig. 1) that solved both of these problems. In this model each neuron inhibits its neighbors and is inhibited by them thus forming a positive feedback loop. This arrangement solves the problem of integrating the signal without the background. When, in Fig. 1, all inputs carry the same signal (the background) all the neurons fire at the background rate and integration does not occur. When the inputs are modulated so that every other neuron has an increased drive and the rest a decreased drive, maximum imbalance occurs in the feedback loops and the modulation is integrated.

More exactly, the line of neurons in Fig. 1 was extrapolated to a continuum and the spatial distribution of inhibition from a neuron at location k to other neurons at distance k_0 was designated $w(k-k_0)$ (Fig. 1, top). Further, afferent inputs to the neuron k arborized to neighboring neurons with strength $v(k-k_0)$ (Fig. 1, bottom). The total synaptic input from afferents and lateral-inhibitory connections were described as convolution integrals in space and the dynamics of an individual neuron were expressed as a first-order rate process with a time constant τ of 0.005 s. This led to the network description reproduced below from Cannon et al. (1983)

$$\tau \frac{\partial x(k,t)}{\partial t} + x(k,t) = \int_{-\infty}^{\infty} v(k-k_0) \cdot u(k_0,t) dk_0 - \int_{-\infty}^{\infty} w(k-k_0) \cdot x(k_0,t) dk_0 . \quad (1)$$

$x(k,t)$ is the firing rate or output of the cell at location k at time t and $u(k,t)$ is the input which is also a function of space and time. The behavior of this equation was examined in the spatio-temporal frequency domain by performing the Laplace transform in time and Fourier transform in space to yield

$$\frac{X(P,s)}{U(P,s)} = \frac{V(P)}{s\tau + 1 + W(P)} = \frac{\dfrac{V(P)}{1+W(P)}}{s\left(\dfrac{\tau}{1+W(P)}\right)+1}, \quad (2)$$

where s represents the complex temporal frequency and P represents spatial frequency. This equation is that of a leaky integrator with a time constant, at any particular spatial-frequency, of

$$T_n(P) = \frac{\tau}{1+W(P)}. \quad (3)$$

When $w(k)$ is adjusted correctly $W(P)$[1] can be brought close to -1 so that T_n rises to 20 s as desired.

Throughout the brain-stem oculomotor system, signals occur in push-pull. If the innervation of the lateral rectus muscle is increased, that of the medial is invariably decreased. The simplest example of this is the vestibulo-ocular reflex. When the head turns to,

1 By convention, lower case letters (x, u, w, v) refer to functions of space and/or time, whereas upper case letters (X, U, W, V) denote the corresponding functions in the spatial and/or temporal frequency domain

say, the left, the discharge rate of left canal afferents increases, those on the right decrease. This push–pull scheme is carried throughout this reflex from sensory input to motor output. Thus, one may imagine, in regarding Fig. 1, that the inputs u_1 and u_2 are relayed from the left and right semicircular canals. The way in which these push and pull signals interweave in the network determines the spatial frequency, P, of interest. If u_1 distributed equally to all cells, its spatial frequency, P, would be 0. If the push–pull inputs alternated and contacted every other cell, as shown in Fig. 1, P has the highest value possible of 0.5 cycles/cell or π radians/cell. Thus P can vary from 0 to π. In Fig. 1, the background, which comes equally to all cells, has a frequency P of zero while the push–pull signal has a value of π.

The time constant in Eq. (3) when P equals 0 or π depends on the form of $w(k-k_0)$. A wide Gaussian was chosen with a narrow central dip as shown in Fig. 1. It was adjusted so that its Fourier transform, $W(P)$, was such that $W(0)$ was approximately 5 and $W(\pi)$ was -0.99975. Consequently $T_n(\pi)$ equalled 20 s and the push–pull signal was integrated, whereas for the background signal, $T_n(0)$ was approximately 0.0008 s and the background was merely passed through with no integration.

Another important attribute of this large, distributed network was increased robustness; the performance of the integrator was not adversely affected by independent, random, band-limited alterations or distortions of the inhibitory profiles, $w(k)$. Integration was relatively preserved even after destruction of 3% of the cells in the network.

The previous study was concentrated specifically on these two major problems – robustness and separation of signal from background – resulting in a rather unphysiological network of identical neurons firing at identical rates. The present paper modifies the earlier model to simulate three additional physiological properties of the neural integrator of the oculomotor system. First, the background firing rate of the input was assumed previously to be equal for every afferent. The actual range of background rates for vestibular afferents extends from about 50 to 150 spikes/s. Since the previous network integrates local differences in afferent firing rate (e.g., the push–pull signal) how might the network distinguish variations in the background rate of neighboring neurons (a signal not to be integrated) from variations due to push–pull signals that should be integrated? Second, single unit recordings from the vestibular nucleus in alert monkeys suggest that different regions of the integrator might receive eye-velocity commands unequally from separate oculomotor subsystems: vestibular, saccadic, and smooth pursuit (Tomlinson and Robinson 1984). Yet all cells in the network are observed to respond at once with the integral of any velocity command. How does the eye-position signal spread so quickly throughout the network? Finally, most premotor, brain-stem neurons that carry the eye-position signal also modulate their firing rates in proportion to eye velocity. Somehow the eye-velocity and eye-position commands are combined within the network. A double-layer network consisting of a population of inhibitory and excitatory cells is shown to respond in this manner.

2 Variation in Background Firing Rates

Experiments have shown that the background firing rates of vestibular afferents have an average of about 100 spikes/s. Neurons in the vestibular nuclei, now believed to form, in part, the neural integrator, have similar background rates. Consequently, the steady-state gain in Eq. (2) for the background should be 1.0. This may be compared to the eye-position modulation on these cells which has a typical coefficient of 2.0 (spikes/s)/deg. This requires that at high temporal frequencies (e.g., 0.1–1.0 Hz) the transfer function for the modulation should be $2/s$ or, since T_n under those conditions is 20 s, the numerator in Eq. (2), right, should equal 40, the steady-state gain for the modulated signal when s equals zero.

In our previous analysis (Cannon et al. 1983) the background rate was assumed to be the same for each afferent which meant that this signal was contained entirely at a spatial frequency P of zero. We demonstrated that an afferent profile, $v(k)$, could be chosen such that for the background input U_b and output X_b,

$$\left.\frac{X_b(P,s)}{U_b(P,s)}\right|_{\substack{P=0\\s=0}} = \frac{V(0)}{1+W(0)} = 1\,, \tag{4a}$$

while for the push–pull modulation,

$$\left.\frac{X(P,s)}{U(P,s)}\right|_{\substack{P=\pi\\s=0}} = \frac{V(\pi)}{1+W(\pi)} = 40\,. \tag{4b}$$

Now, however, one must consider the case in which there is spatial variability in the background so that $U_b(P,s)$ may be non-zero for values other than P equal to zero. Since the background changes, almost by definition, very slowly with time if at all, we need only consider the steady-state case where s is zero,

$$\left.\frac{X_b(P,s)}{U_b(P,s)}\right|_{s=0} = \frac{V(P)}{1+W(P)}\,. \tag{5}$$

Experiments indicate that variations in the background firing rate from one afferent to another are about the same as among the putative neurons of the integrator so this is one design goal. Further, the sum

of background inputs from all left afferents (u_1, Fig. 1) must equal that from the right (u_2), otherwise the difference would be correctly interpreted as a push–pull modulation and integrated accordingly. If the difference ($u_{b1}-u_{b2}$) persisted, as in a unilateral vestibular lesion, the output of the integrator would attempt to rise, or fall, by the steady-state value, $40\cdot(u_{b1}-u_{b2})$, according to Eq. (4b). This would not be allowed, of course, since, as the eye began to move in response to this command, pulses of activity from burst neurons would create quick phases and periodically reset the eye and the neural integrator, creating the eye-movement pattern known as vestibular nystagmus.

Consequently, while the background rate may vary from one afferent to another, the difference between the sum over all the push and that over all the pull afferents must, in the normal case, be zero. Put another way, if the difference were not zero, then the background rate would have a significant component at a spatial frequency of P equal to π. To prevent this, the spatial variability in $U_b(P)$, then, may be assumed not to contain components at π. Figure 2a shows such a distribution for a network of 32 cells – a convenient-sized network utilized to test many of these ideas. Cell 32 is a neighbor of cell 1 to eliminate edge effects. The average background rate for the push (odd-numbered) and pull (even) afferents equals 100 spikes/s so that $U_b(\pi)$ is zero. Individual rates within each push and pull pool were chosen randomly from a Gaussian distribution.

The problem created by this input variability is illustrated by the open circles in Fig. 2d which shows the output generated by the network proposed by Cannon et al. (1983) in response to the input of Fig. 2a. Local spatial variations in the background rate will stimulate the local feedback loops and will be partially integrated which in turn causes these variations to become exaggerated in the background rates of the neurons of the network. This amplification can be seen graphically in Fig. 2b which is similar to the analysis of Cannon et al. (1983). As in Fig. 3 of that paper, $w(k)$ (recall Fig. 1) is represented by a positive Gaussian curve with the central notch represented by a negative impulse as shown in the legend of Fig. 2b. The curve $v(k)$ (recall Fig. 1) is also represented by a Gaussian given in the legend of Fig. 2b. These choices lead to functions $W(P)$ and $V(P)$, also given in the legend of Fig. 2b, that, from Eq. (2), create the surface in Fig. 2b. The front edge of this surface, at P equal to zero, is the Bode diagram of the gain $|X/U|$ of the background if its spatial frequency content is zero (as in our previous, idealized case). The back edge is the Bode diagram for the push–pull signal which contains non-zero spatial harmonics only at P equals π. It is the Bode diagram of a leaky integrator with a time constant of 20 s. The left edge shows the steady-state response to the background (s essentially zero) if it has spatial frequency components other than zero. The gain rises from 1.0 to 40. It is this rise in gain that reflects local, partial integration of local variations in the afferent background that would cause the variations in the background of the network's cells to become unrealistically large as illustrated in Fig. 2d by the open circles. Thus, the network formerly proposed by Cannon et al. (1983) does not work correctly when there is spatial variation in the afferent background rates.

Fig. 2A–D. Improvement in the model response for the case of variable background firing rates. **A** Background firing rates chosen for the afferents for a 32-neuron network as a function of space. The average background firing rate for the "push" (odd-numbered) and "pull" (even-numbered) afferents each equal 100 spikes/s which makes $U_b(\pi)$ equal to 0. However, within each pool of "push" or "pull" afferents the firing rate is Gaussianly distributed about the mean in a random fashion. **B** Amplitude of the transfer function $\frac{X(P,s)}{U(P,s)}$, using our previous form (Cannon et al. 1983) of $w(k)$ and an appropriately scaled $v(k)$ such that

$$\frac{X(0,0)}{U(0,0)}=1 \quad \text{and} \quad \frac{X(\pi,0)}{U(\pi,0)}=40.$$

Temporal frequency increases logarithmically from 10^{-3} to 10^{+5} rad/s along the ω-axis. Spatial frequency increases arithmetically from 0 to π along the P-axis. Amplitude increases logarithmically on the vertical axis. Spatial frequency content of the assumed inhibitory and afferent profiles are

$$w(k)=A_{w1}e^{-\frac{1}{2}(k/\sigma_w)^2}-A_{w2}\delta(t) \;\rightarrow\; W(P)=A_{w1}\sigma_w\sqrt{2\pi}e^{-\frac{1}{2}(P\sigma_w)^2}-A_{w2}$$

$$v(k)=A_v e^{-\frac{1}{2}(k/\sigma_v)^2} \;\rightarrow\; V(P)=A_v\sigma_v\sqrt{2\pi}e^{-\frac{1}{2}(P\sigma_v)^2},$$

where A_{w1} is 1.0, A_{w2} is 0.999807, σ_w is 1.5, A_v is 1.369, and σ_v is 1.095. Notice that with σ_w greater than σ_v, $\left|\frac{X(P,s)}{U(P,s)}\right|$ grows steadily with spatial frequency, P, for small values of s. **C** Gain of the same network as in **B**, but with new values for the assumed synaptic weighting profiles. The form of each profile is the same as in **B**, but the new parameter values are: A_{w1} equal to 4.0578; A_{w2}, 1.00976; σ_w, 1.2; A_v, 4.0539; σ_v, 1.2. Notice that when σ_w equals σ_v, the gain remains low in the spatial-frequency plane for small values of s until P reaches π. **D** Output background firing rate as a function of space in response to the afferent background firing rates in **A**. Open circles show the response using the parameter values in **B**, and closed circles correspond to the response for the parameter values used in **C**

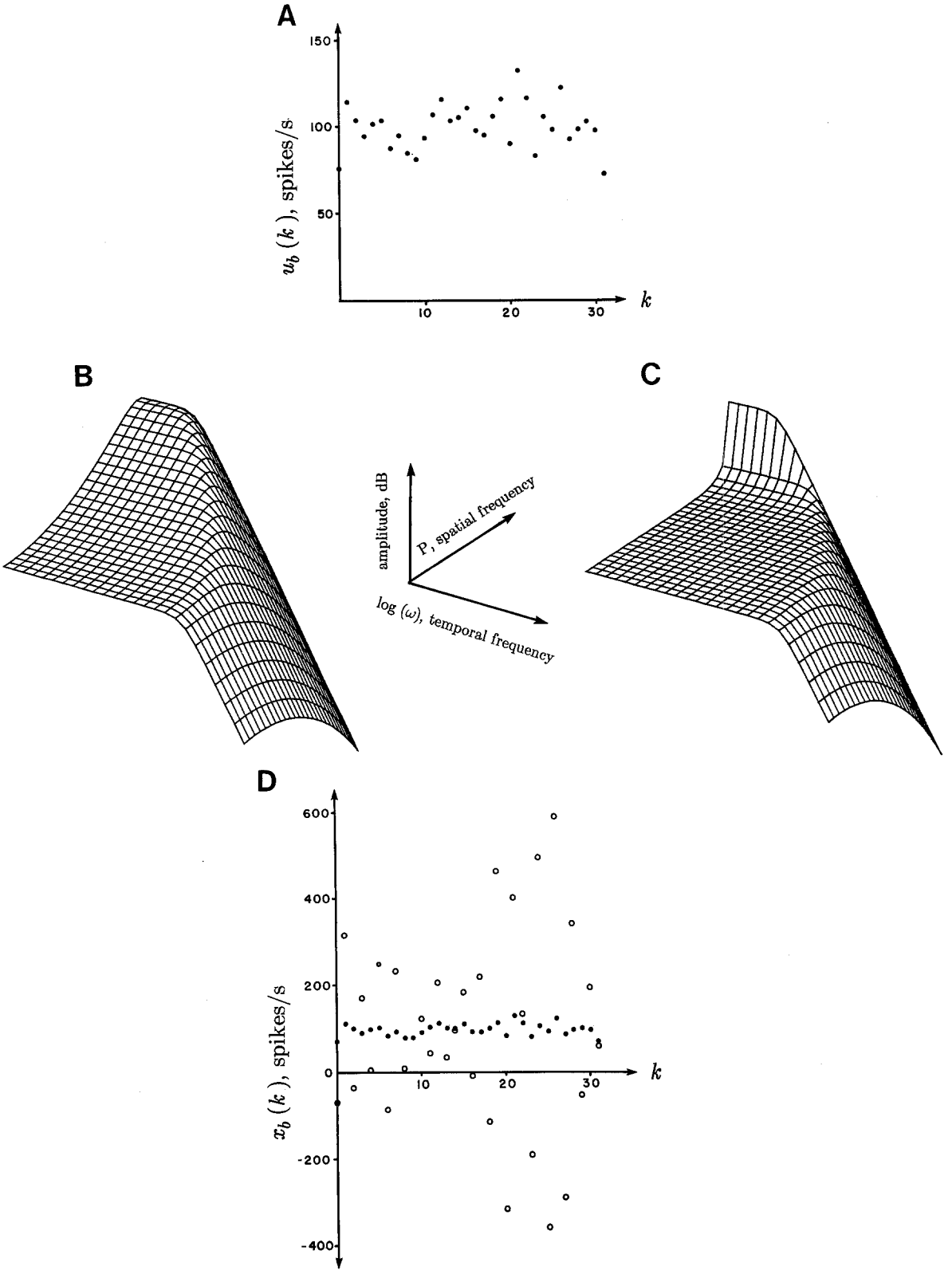
A
150
100
50
$u_b(k)$, spikes/s
10
20
30
k
B
C
amplitude, dB
P, spatial frequency
log (ω), temporal frequency
D
600
400
200
0
-200
-400
$x_b(k)$, spikes/s
10
20
30
k

The solution to this problem, shown in Fig. 2c is to prevent the steady-state gain (left edge) from rising for all P less than π; that is, we want

$$\frac{X_b(P)}{U_b(P)} = \begin{cases} 1.0 & \text{if } |P| < \pi \\ 40 & \text{if } |P| = \pi \end{cases} \quad (6)$$

Since, by the physiological constraint that $U_b(P)$ equal 0 when P equals π, Eq. (6) will insure that $X_b(P)$ equal $U_b(P)$ for all values of P. Thus, the spatial variations in background within the network, $x_b(k)$, will equal the spatial variations in the background of the afferents $u_b(k)$, as observed experimentally.

The surface in Fig. 2c may be realized by manipulating the profiles of $v(k)$ and $w(k)$ so that the gain in Eq. (5) remains near 1.0 for all P less than π. This only requires that v and w be chosen so that $1 + W(P)$ be nearly equal to $V(P)$ for all P less than π. This can be done by making the variances in the Gaussian profiles for $w(k)$ and $v(k)$ the same. Then, with proper amplitude scaling, $1 + W(P)$ and $V(P)$ will be equal for most P so that, as in Eq. (6), their ratio will be 1.0. As P becomes very close to π, however, $1 + W(P)$ becomes very close to zero (to satisfy Eq. (3)) while $V(P)$ remains a small positive number. Their ratio thus shoots up to a large value at π as desired by Eq. (6). The specific profiles for $v(k)$ and $w(k)$ are given in the legend of Fig. 2c and the resulting values of $W(P)$ and $V(P)$ produce the surface in Fig. 2c. This network still integrates the push–pull signal with a time constant of 20 s but now has a gain of 1.0 for the background and its spatial variability as well.

A comparison between the response of the former and new versions of our model to variable background rates on a 32-neuron network is shown in Fig. 2d. The background rates were distributed as shown in Fig. 2a. As already mentioned, the earlier version of the network, shown in Fig. 2b, which was not designed to cope with variable background firing rates, amplifies the higher frequency fluctuations in those rates (open circles). In contrast the output firing rates, filled circles, for the new version of the model illustrated in Fig. 2c are virtually identical to the input background rates shown in Fig. 2a. The crucial feature was choosing the variances of the Gaussian distributions in $v(k)$ and $w(k)$ to be equal (they need not be identical) so that $X_b(P)/U_b(P)$ has the form of a steep-edged, high-pass, spatial filter that has a low gain (1.0) for all P smaller than π.

3 Response to Local Push–Pull Inputs

Every brain-stem neuron that carries an eye-position signal, modulates its firing rate in relation to eye position for every type of eye-movement, regardless of whether it was of vestibular, optokinetic, pursuit, or saccadic origin. Most of these neurons also carry eye-velocity information. However, unlike the position signal, the eye-velocity component of the firing rate is not independent of the type of eye movement. For example some neurons in the vestibular nucleus carry eye-position information for all types of eye movements, yet carry an eye-velocity component only during smooth pursuit movements (so-called "position" neurons of Tomlinson and Robinson 1984). Others modulate their firing rates with eye position for all eye movements but with eye-velocity only for pursuit and vestibular eye movements ("position-vestibular cells", *ibid*). Still others carry saccadic eye-velocity information. To account for this, these authors postulated that an eye-velocity command for one particular type of eye movement projects in push–pull to only a part of the integrator pool. Cells in the immediate vicinity might then modulate with that type of eye velocity whereas more distant cells would not. By definition, of course, all cells in the pool carry the eye-position signal. The goal of this section is to investigate if and how the eye-position modulation can spread spatially to all the outputs of the neural integrator even though the input arrives on only a local region of the total network.

This investigation will, however, not be brought to completion because it would still result in a model in which the neurons carried the eye-position signal but not the velocity signal. To deal with that, a double-layer model will be presented in the next section, and it will be demonstrated to solve both problems – its cells will carry both an eye-velocity and eye-position signal and the latter will appear everywhere in the network even when the former is seen in only part of it. Nevertheless, the double-layer network is more complex and difficult to understand so it is worth examining the simpler model (Fig. 1) to see the nature of the problems created by local inputs and their solutions, since they apply in general to the more complex model.

Since we are concerned with the *spatial* transformation of a local input into a global output, it is simplest to begin by examining the network response under steady-state conditions. Consider an idealized push–pull input of amplitude 1.0 present only on afferents 8 to 23 of a 32 neuron network as shown in Fig. 3a.

If the integral of the input spread uniformly throughout the whole network, each cell would have modulated, alternately, up or down by 40 [Eq. (4b)]. The transform, $X(P)$, of this state would be a pair of impulses with amplitude 1280 (equal to 32×40) at frequencies P of π and $-\pi$. This then is the desired output. The amplitude spectrum of the input, on the other hand, is shown in Fig. 3b and has the form of the so-called Fourier-series kernel centered at $|P|$ equal π

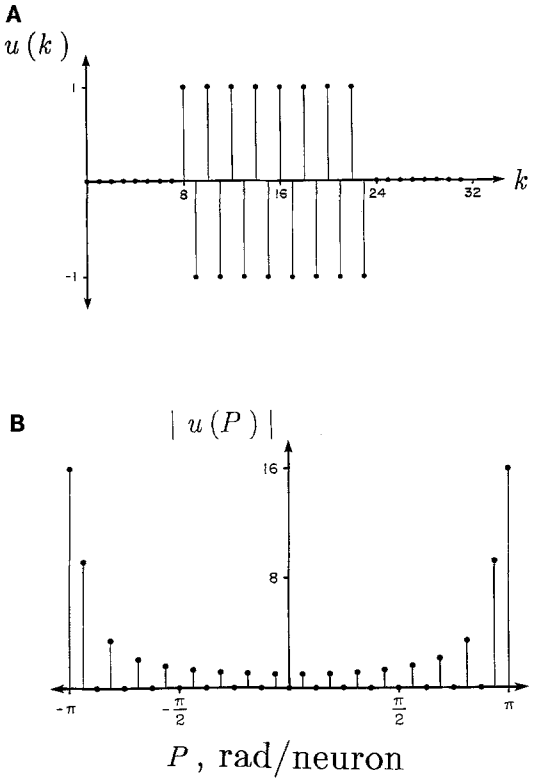

Fig. 3A and B. Local, push–pull input and its Fourier transform. **A** Unity-amplitude, push–pull input, $u(k)$, present on afferents 8–23 of a 32-neuron network. **B** Spatial-frequency content of the input signal of **A**. The spectrum is the amplitude of the discrete Fourier transform of the input, and takes the shape of a full-wave rectified Fourier series kernel, centered about $|P|$ equal to π. By comparison, the spectrum of a unity-amplitude, push–pull, input signal distributed across the entire network is a pair of impulses with amplitude 32 at $|P|$ equal to π

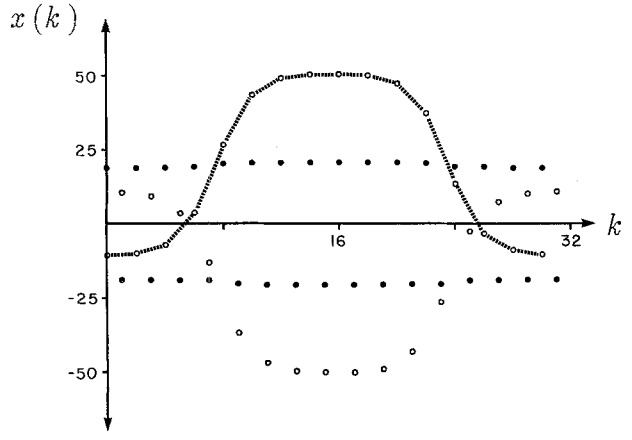

Fig. 4. Change in steady-state firing rate, $x(k)$, in response to the local, push–pull input of Fig. 3. Open circles illustrate the network response using our former choice of parameters as listed in Fig. 2b. The responses of the "push" outputs are connected by the dashed line to emphasize the spatial profile of the steady-state output. Filled circles show the steady-state response of the network with the improved parameter choices listed in Fig. 2c

(Papoulis 1962).[2] To transform the spectrum of the input to that of the desired output, the network must attenuate all spatial frequency components in $U(P)$ except where $|P|$ equals π. Therefore, just as was required for the solution to the problem of the variable background firing rate, $X(P)/U(P)$, in steady state (s equal to zero), must have the form of a steep-edged, spatial filter mainly passing only the components at π.

To demonstrate the similarity of the solutions to both the variable background firing rate and the partial input problems, the same choices of $v(k)$ and $w(k)$ used in Fig. 2b and c were used to generate the steady-state responses shown in Fig. 4. The input was the push–pull signal in Fig. 3. The open circles show the steady-state response of our earlier model, with the transfer function illustrated in Fig. 2b, for which the problem of partial inputs had not been considered. Since our previous model did not behave like a spatial filter sharply cutting off values below π, the side lobes of the amplitude spectrum of the input (Fig. 3b) are not attenuated sufficiently and the output is not distributed evenly in space. Integration occurred mainly for cells 8 to 23 but not elsewhere. Even worse, the other neurons integrated in the wrong direction. Conversely with the new forms of $v(k)$ and $w(k)$ given in the caption of Fig. 2c, the spatial selectivity of the network at π is sufficiently sharp that the side bands of $U(P)$ in Fig. 3b are attenuated and the push–pull output is spread approximately equally to every neuron as shown by the filled circles in Fig. 4. Thus the same filter characteristics that allow the network to handle spatial variations in the background rates of the afferents also allow the network to spread the integrated, push–pull signal throughout the network even though it is supplied only to a part. The basic principle is that if the background had a spatial frequency content only at zero, and the push–pull input only at π, then it would not matter what the network did for intermediate values of P. Both problems were caused by backgrounds and signals which spilled over into the intermediate zone. Reshaping the network so as not to amplify any spatial frequency components in between zero and π solved both problems.

If one still wants the steady-state output of the integrator to be 40 for a unit velocity input on N_{on}

2 In the continuous space domain the Fourier transform of such a partial, push–pull input is the familiar sinc function, $\frac{2\sin(PT)}{P}$, centered about $|P|$ equal to π, where T equals half the width of the partial input. The transition from continuous to discrete space introduces aliasing which distorts the amplitude spectrum such that the amplitude decreases less rapidly than the sinc function as P departs from π as specified by the Fourier-series kernel, $\frac{\sin(P[T+\frac{1}{2}])}{\sin(P/2)}$

afferents out of N total, the gain $-\frac{40}{(N_{on}/N)}-$ must be increased to 80 since N_{on}/N is $\frac{1}{2}$ in the example in Fig. 3a. Such a change was not made in the simulation for Fig. 4 because we wanted a direct comparison of the results of chosing the $w(k)$ and $v(k)$ used in Fig. 2b and c. Consequently the amplitude of the output (20 units, filled circles, Fig. 4) is only half the desired value. The changes required in $v(k)$ and $w(k)$ to make $X(\pi)/U(\pi)$ equal 80 while keeping $X(P)/U(P)$ approximately 1.0 for P other than π would require only trivial adjustments of $W(P)$ and $V(P)$.

The analysis thus far has been for the steady-state case. How fast does the integrated signal spread throughout the network? For the steady-state case the numerator, $V(P)$, and the denominator, $1+W(P)$, of the new transfer function were approximately equal so that $X(P)/U(P)$ equaled 1.0 for P less than π. As P became close to π, $1+W(P)$ became close to 0 so that the ratio suddenly became a large number as required by Eq. (6). For time-varying inputs the temporal frequency component of the input is no longer zero and the magnitude of s may be large compared to $1+W(\pi)$. This means that the magnitude of $X(P,s)/U(P,s)$ does not retain steep-edged, highpass characteristics in the spatial frequency plane when the temporal frequency is high as shown in Fig. 2c. The result is that the integrated, push–pull output can not spread instantaneously in time over the entire network for the case of a time-varying input presented on a local region of afferents. With the parameters used for the new forms of $v(k)$ and $w(k)$ given in the caption of Fig. 2c, it takes approximately 1 s before the outputs for a step input become distributed across the entire network. The sources of this transient are the spatial frequency components of $U(P)$ for values of P slightly less than π shown in Fig. 3b. These cause higher spatial-frequency components of the output (P still less than π) that decay more slowly with time which is reflected by the relatively low temporal corner frequencies on the surface in Fig. 2c when P is slightly less than π. For example the component at $(\frac{31}{32})\pi$ has a time constant of 1.58 s. Such components slow the spread of the integrated signal.

Two mechanisms could be invoked to reduce this effect. If the input were not restricted to only one large region, but were instead broken up into smaller ones, then the first non-zero harmonic of $U(P)$, as P decreases from π, would occur at a lower spatial frequency. All such undesired harmonics of $U(P)$ would occur at lower spatial frequencies with higher temporal corner frequencies on the $X(P,s)/U(P,s)$ surface of Fig. 2c which in turn means that all the transients in the spread of $x(k,t)$ would decay more rapidly. A second mechanism, that could be invoked simultaneously, would be to choose the spatial spread of $v(k)$ to be larger than that of $w(k)$ so that the gain of $X(P)/U(P)$ is not just 1.0 for values of P between 0 and π as in Eq. (6) but is less than 1.0. This scheme would further attenuate the gain of the undesired side lobes of $U(P)$ so that $X(P)$ would, for all values of s, be a better approximation of the ideal output spectrum; that is, an impulse when $|P|$ equals π with no other spatial-frequency components.

Although these changes could improve the single-layer model of Fig. 1, they were not pursued because the problem of rapidly distributing the eye-position command throughout the network is remedied for the case of the double-layer network presented in the next section. The temporal nature of distributing the integrated output was detailed for the single-layer model because the source of this potential problem and the means of preventing it from becoming significant are more easily demonstrated with the simpler, single-layer network.

4 A Double-Layer Network: Feed-Forward Velocity Plus Eye-Position Information

Most models of premotor circuits describe the overall signal processing of the oculomotor system and are not intended to represent actual anatomical pathways. This approach has led to the diagram of Fig. 5 which shows a separate, feed-forward, velocity pathway, weighted by r, and the integrated pathway, weighted by K, to account for the eye-velocity and eye-position dependency of a motoneuron's firing rate. If this block diagram corresponded to anatomical pathways, then one would expect to record frequently from neurons whose firing rates modulated only with eye-position; i.e., neurons at the output of the neural integrator. However, pure position neurons have been observed only relatively infrequently (Keller 1974). Further, the lesion experiments of Cannon and Robinson (1985) and Cheron et al. (1985) indicate that the integrator lies in part in the medial vestibular nucleus while the study of Tomlinson and Robinson (1984) shows that the neurons there that carry the eye-position signal, and so are likely to be part of the integrator, also carry an eye-velocity signal. Moreover, the cells must be able to carry an eye-velocity signal for some types of eye-movements but not others.

This section demonstrates that a double-layer network, one consisting of inhibitory and the other of excitatory cells, can perform all of the signal processing required to create the eye-position command and combine it with the feed-forward velocity signal. The lateral inhibition enables the push–pull command to be integrated independently of the background firing rate, and the excitatory layer adds a velocity feed-

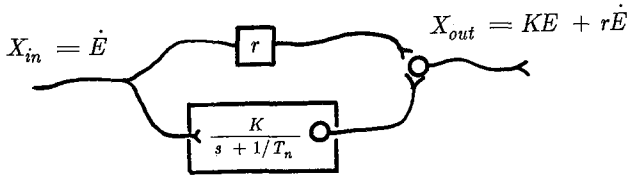

$$\frac{X_{out}}{X_{in}} = r + \frac{K}{s + 1/T_n} = r \left\{ \frac{s + (\frac{K}{r} + \frac{1}{T_n})}{s + 1/T_n} \right\}$$

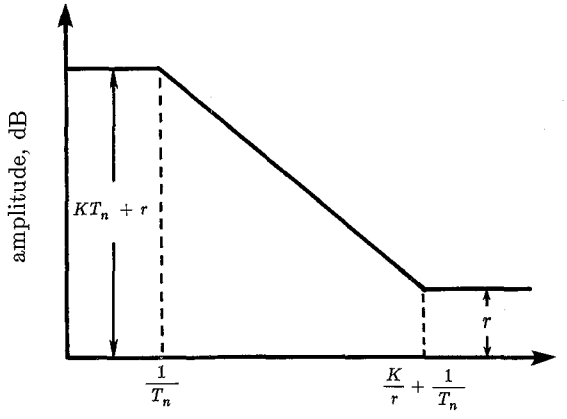

Fig. 5. Wiring diagram and Bode plot illustrating the overall signal processing required to convert an eye-velocity signal to an eye-velocity plus position command with each component weighted by r and K, respectively. The integrator which generates the eye-position command is not ideal; rather it leaks with a time constant of T_n equal to 20 s. The transfer function for this network has a pole when s equals $\frac{-1}{T_n}$ and a zero when s equals $-(K/r + 1/T_n)$. The Bode plot shows the log of the amplitude response of this network as a function of the log of the temporal frequency of the input. Experimental evidence shows that neurons in the integrator must individually conform quantitatively to this general form

forward mechanism so that the outputs also carry the eye-velocity signal. The transfer properties required of the network are defined in Fig. 5. In order to generate the eye-position component, there must be a (temporal) pole at s equal to $-1/20$ or 0.05 rad/s; just as was required in the single-layer network. The location of a high-frequency zero, when s equals, primarily determines the relative weighting of the position and velocity components of the output. Typically K is approximately 2.0, r is on the order of 1.0, and T_n is, as before, 20 s

For the most general case of a double-layer network, shown in Fig. 6, the afferents could project to both layers, there could be connections within each layer, and each layer could project to the other one. The coupled equations for the continuum description of each layer are

$$\tau_e \frac{\partial x_e(k,t)}{\partial t} + x_e(k,t) = v_e(k) * u(k,t) + w_{ee}(k) * x_e(k,t) - w_{ei}(k) * x_i(k,t), \quad (7a)$$

$$\tau_i \frac{\partial x_i(k,t)}{\partial t} + x_i(k,t) = v_i(k) * u(k,t) - w_{ii}(k) * x_i(k,t) + w_{ie}(k) * x_e(k), \quad (7b)$$

where * indicates the spatial convolution operator. As before, $x(k,t)$ refers to neuronal output firing rate as a function of space and time with subscripts e and i denoting excitatory and inhibitory layers, respectively. The $v(k)$'s are the weightings of the input projections to each layer, $w_{ee}(k)$ and $w_{ii}(k)$ are the intra-layer projections, and $w_{ei}(k)$ and $w_{ie}(k)$ are the inter-layer projections.

Since a particular afferent must obey Dale's law (i.e., it's either excitatory or inhibitory, but not both), and $v_e(k)$ and $v_i(k)$ refer to collateralizations of the same afferent to each layer, then either $v_e(k)$ and $v_i(k)$ are both negative (inhibitory afferents) or both positive (excitatory afferents), but not mixed in sign. $w_{ei}(k)$ and $w_{ii}(k)$ denote the projections from the inhibitory cells to the excitatory and inhibitory cells, respectively, and with the sign convenciton in Eq. (7a) and (7b) (notice the minus signs), both of these profiles must be greater than or equal to zero for all values of k. Similarly $w_{ie}(k)$ and $w_{ee}(k)$ describe the profiles of the projections from the excitatory cells to the inhibitory layer and excitatory cells, respectively, and must also be greater than or equal to zero. Inhibitory neurons may be intrinsically different from excitatory ones, so we arbitrarily chose τ_i equal to 0.008 s and τ_e equal to 0.005 s.

Taking the Laplace transform with respect to time and the Fourier transform in space for Eq. (7a) and (7b), and solving for $X_e(P,s)/U(P,s)$ and $X_i(P,s)/U(P,s)$, yields

$$\frac{X_e(P,s)}{U(P,s)} = \frac{V_e(P)[s\tau_i + 1 + W_{ii}(P)] - W_{ei}(P)V_i(P)}{[s\tau_e + 1 - W_{ee}(P)][s\tau_i + 1 + W_{ii}(P)] + W_{ei}(P)W_{ie}(P)}, \quad (8a)$$

$$\frac{X_i(P,s)}{U(P,s)} = \frac{V_i(P)[s\tau_e + 1 - W_{ee}(P)] + W_{ie}(P)V_e(P)}{[s\tau_e + 1 - W_{ee}(P)][s\tau_i + 1 + W_{ii}(P)] + W_{ei}(P)W_{ie}(P)}. \quad (8b)$$

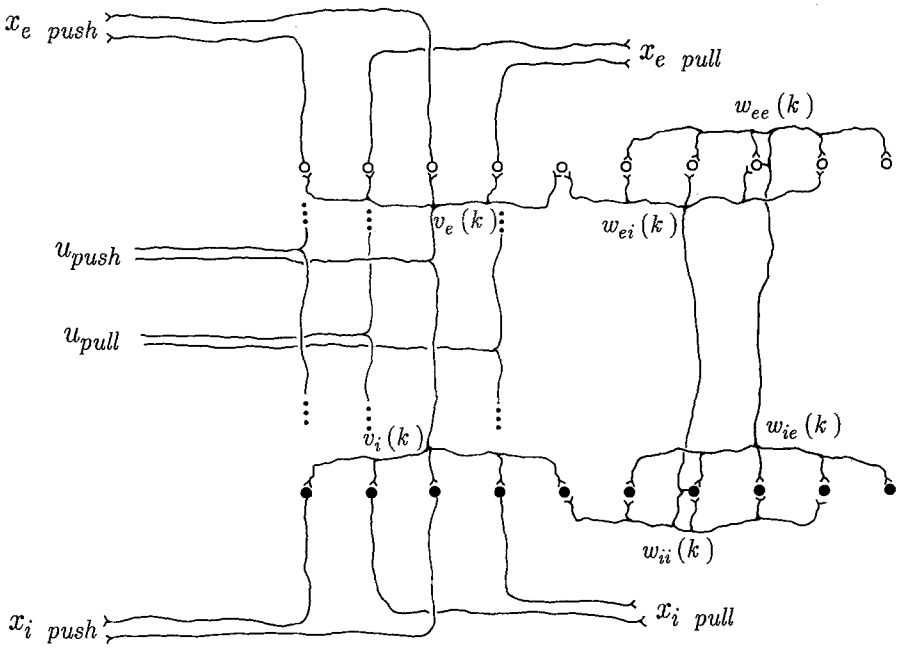

Fig. 6. Schematic representation of a double-layer network. For convenience of description, the inhibitory cells (filled neurons) and excitatory cells (open neurons) are grouped separately into two layers. The projections on the left side depict the input and output connections of the network. The "push" and "pull" afferents are highly interdigitated, just as was assumed for the single-layer model. Their primary projection is to every other neuron. The arborization for only one "push" afferent is illustrated, but of course, each afferent, both "push" and "pull", arborizes to both excitatory and inhibitory cells with synaptic-weighting profiles $v_e(k)$ and $v_i(k)$, respectively, as suggested by the dots. The intranetwork collateralizations are illustrated once for each class of projection on the right side. The afferent arborizations and intra-network collateralizations are repeated for every afferent and neuron throughout the entire network, and are separated in this figure merely for reasons of clarity

Equations (8a) and (8b) have the same pair of temporal frequency poles but different zeros. In order to retain an integrator time constant of 20 s when P equals π, one pole must be located where s equals $-1/20$. Recall from Fig. 5 that only this one pole is required to achieve integration. The nature of the model, however, makes it impossible to add a zero without also including an additional pole. Fortunately it is easy to push this pole to such high temporal frequencies that it lies outside the bandwidth of the signals with which the network must deal. Both the inhibitory and excitatory cells serve as outputs for the double-layer model and therefore, the eye-velocity as well as the eye-position signal must be present on both cell types. Thus, the zero must be retained in both Eqs. (8a) and (8b). If v_e or v_i were zero, this feature would be lost. Further, if, for example, v_i were zero, the zero in Eq. (8a) would be fixed at $-(1+W_{ii}(\pi))/\tau_i$, a value much too large (375 rad/s) to be useful. A similar problem occurs if v_e were zero. For these reasons we postuled that the input projects to both layers. With these conditions it appears to be qualitatively possible for the transfer function of Eqs. (8a) and (8b) to reproduce the desired Bode plot shown in Fig. 5 at the important spatial frequency when P equals π. The remaining question is, can a physiologically reasonable set of synaptic profiles be chosen for $v_i(k)$, $v_e(k)$, $w_{ee}(k)$, $w_{ii}(k)$, $w_{ie}(k)$, and $w_{ei}(k)$ so that $X(\pi, s)/U(\pi, s)$ resemble the Bode plot in Fig. 5 to a reasonable degree of accuracy for both layers *simultaneously*. Because of the many degrees of freedom now available, we shall demonstrate the feasibility of this network only with a specific example.

We have chosen to simulate simultaneously two classes of neurons in the vestibular nucleus – position (P) and position-vestibular (PV), reported by Tomlinson and Robinson (1984) – with one set of network parameters. The general firing patterns of all such cell types are described by Eq. (9a).

$$R = R_0 + KE(t) + r_p\dot{E}_p(t) - r_v\dot{H}(t) \tag{9a}$$

and for the two specific types, P and PV, by

$$R_P = 70 + 1.1E(t) + 0.4\dot{E}_p(t), \tag{9b}$$

$$R_{PV} = \begin{cases} 70 + 1.1E(t) + 0.4\dot{E}_p(t) \\ \quad \text{for pursuit only} \\ 70 + 1.1E(t) - 1.0\dot{H}(t) \\ \quad \text{for the vestibulo-ocular reflex (VOR)}, \end{cases} \tag{9c}$$

[3]

3 Tomlinson and Robinson were also concerned about whether visual suppression or cancellation of the VOR was done by simultaneous pursuit and vestibular commands. This question concerns events upstream from the neural integrator and lies outside our current interest. The point is only to show that different cells in the network can respond differently to different velocity inputs

where $\dot{E}_p$ and $-\dot{H}$ are eye-velocity commands for pursuit and the VOR respectively, r_p and r_v are their weighting coefficients, K is the eye-position coefficient and R_0 is a background rate. Note that P cells carry no eye-velocity signal for vestibular stimulation. The constraints required to choose the parameters for $v_e(k)$, $v_i(k)$, $w_{ee}(k)$, $w_{ii}(k)$, $w_{ie}(k)$, and $w_{ei}(k)$ along with the specific parameter values are detailed in the Appendix, but several points of broad strategy should be made. Firstly, none of the profiles required a change in sign as a function of k (i.e., Dale's law was obeyed), and none of the degrees of arborization or intensities of synaptic interactions assumed physiologically unrealistic values. Secondly, none of the six profiles could be neglected if the model is to possess the desired transfer properties for both the excitatory and inhibitory cells simultaneously. For convenience, the profiles were again represented by Gaussian distributions. Because of the many degrees of freedom, the choice of parameter values is by no means unique and the Appendix reviews the order in which certain constraints were imposed. Some of the parameters were chosen by trial and error and other choices of profiles could lead to similar results.

As an example of the underdetermination of the model, it was found that four of the six profiles, $w_{ee}(k)$, $w_{ii}(k)$, $w_{ei}(k)$, and $v_i(k)$ could be relegated to delta functions; that is, each cell or fiber need contact itself or one other cell. Thus, most of the behavior was governed by the way inputs distributed to the excitatory layer, $v_e(k)$, and how the excitatory cells distributed to the inhibitory layer, $w_{ie}(k)$. Again, these choices were not mandated but were made to simplify. As a result of these choices, the main positive feedback loop by which this network integrates (Fig. 6) is from the j^{th} excitatory cell to a nearby k^{th} inhibitory cell via w_{ie}, from there to the k^{th} excitatory cell, then back to the j^{th} inhibitory cell, again via w_{ie} and finally back to the j^{th} excitatory cell. This loop causes all cells, excitatory and inhibitory, to excite themselves. Thus both layers share equally in the integration process.

Since both P and PV cells modulate with pursuit velocity, the pursuit afferents were allowed to project directly to all the neurons in the double-layer network. On the other hand, since only the PV cells carry the vestibular, eye-velocity signal, the vestibular afferents projected directly to only the central 16 neurons of each 32-neuron layer (similar to the scheme in Fig. 3a). If the model is successful, the latter 16 neurons will look like PV cells, the rest like P cells. Since r_p does not equal r_v in Eq. (9c), two distinct sets of profiles are required for the pursuit $\{v_e(k), v_i(k)\}_p$ and vestibular $\{v_e(k), v_i(k)\}_v$ afferents. It should be pointed out, however, that only one set of intranetwork connections, ($w_{ee}(k)$, $w_{ii}(k)$, $w_{ie}(k)$, and $w_{ei}(k)$) are required to simulate both classes of neuron. In other words the intrinsic connections of the double-layer are homogeneous. This is a desirable property of the model if it is to be realistic. A local region of this network carries a particular type of eye-velocity signal depending on the regional distribution of afferents, whereas the entire network must carry the eye-position signal and with the same integrator time constant.

The transfer function surface of both excitatory and inhibitory cells, for each type of afferent, using the parameter choices in the Appendix is shown in Fig. 7. Figure 7a and 7b represent the transfer properties of the pursuit components of *both* P and PV cells for the excitatory and inhibitory cells, respectively. Figures 7c and 7d represent the transfer properties of the excitatory and inhibitory cells, respectively, for the vestibular component of the PV cells. Comparison with Fig. 2c shows why the problem of rapidly distributing the eye-position signal for local inputs has disappeared in the double-layer model. In Fig. 2c the Bode diagram when P is equal to π (the back edge) integrates out to arbitrarily high temporal frequencies causing the whole back-right corner of the surface to be pulled down. Consequently the Bode diagram created by cutting this surface at the constant value of P of, say, $(31/32)\pi$ has a low, temporal, corner frequency. This will cause transients created by the side lobes in Fig. 3b (the Fourier transform of a partial input) near π to be slow in propagating the integrated signal uniformly throughout the network. The addition of the velocity signal, or zero, removes the problem. In Fig. 7, the Bode diagram formed by cutting the surface where P equals $(31/32)\pi$ has a high corner frequency. The transients created by the side lobes in Fig. 3b will have very small time constants, on the order of τ_i or τ_e, and the eye-position signal will appear almost instantaneously everywhere in the network.

To illustrate behavior in the time domain, such as one sees when recording from brain-stem neurons, we calculated the network response for one cycle of a triangular-wave, pursuit movement followed by a brief on-off step of constant-velocity head rotation in darkness. The inputs on the odd numbered afferents are illustrated in Fig. 8a[4]. The even numbered inputs would be a mirror image of these waveforms relative to the background firing rate and are omitted for clarity. Figure 8b shows the network response for the odd-numbered, excitatory and inhibitory outputs using the parameter values listed in the Appendix. During the pursuit movement, every output carries a

4 For reasons of graphical clarity the background firing rates of all the afferents are identical. A broad distribution of background firing rates such as those of Fig. 2, could have been used and each cell would have simply had a different background firing rate

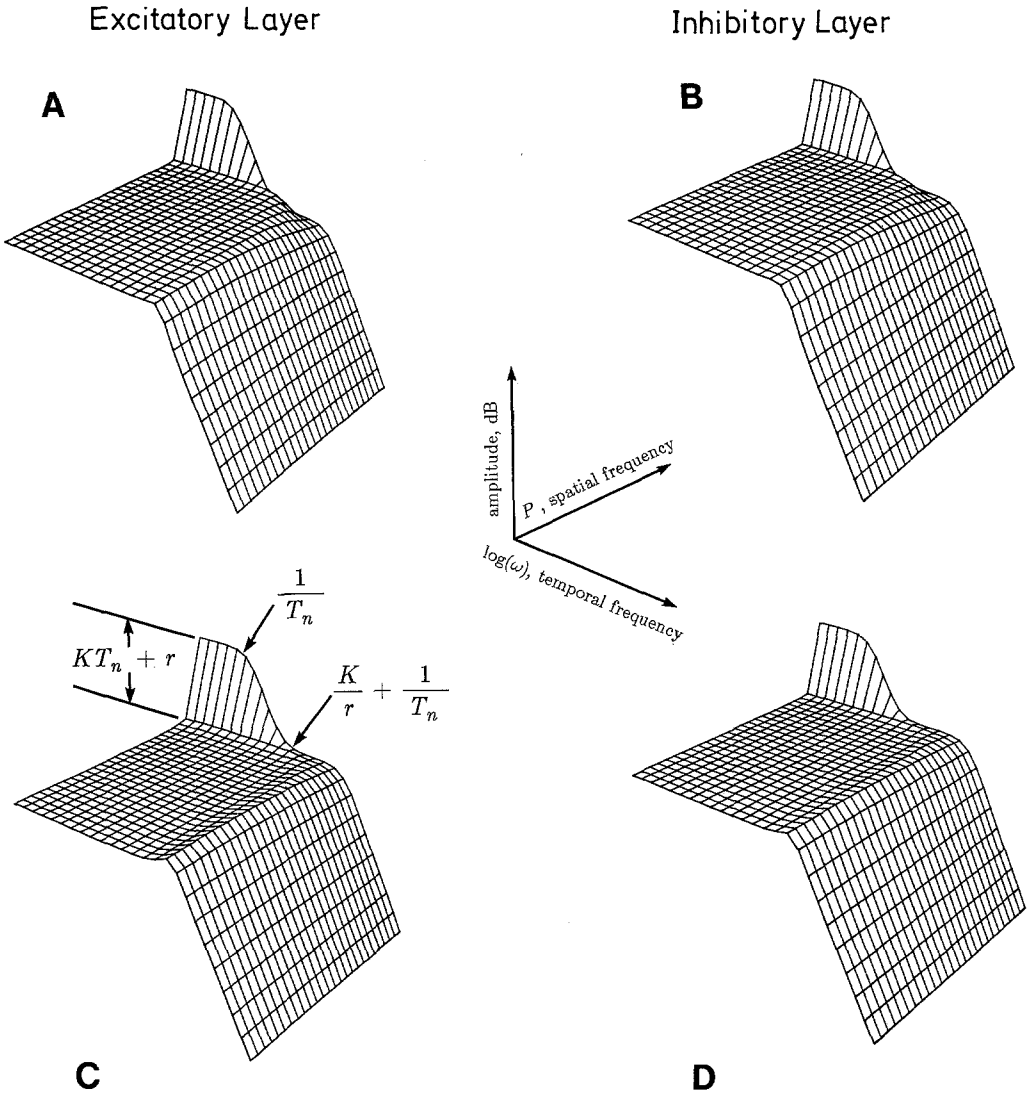

Fig. 7A–D. Gains of the transfer function of the double-layer model for pursuit (**A** and **B**) and vestibular (**C** and **D**) afferents. **A** and **C** are the responses for the excitatory layer, while **B** and **D** are for the inhibitory cells. Compare the highest spatial-frequency plane (for which P equals π) to the Bode plot of Fig. 5. The axes are the same as those of Fig. 2b and c

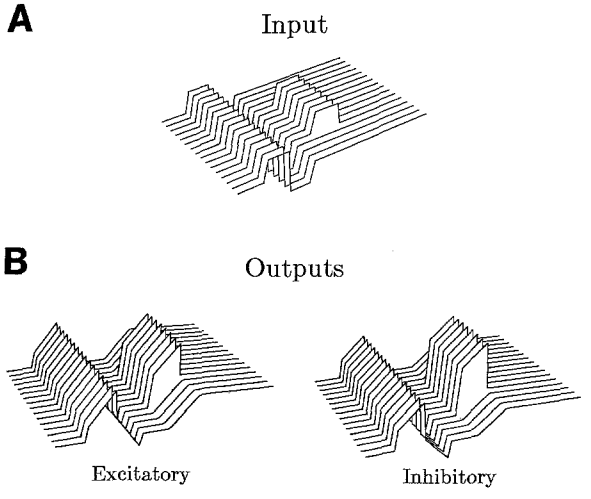

◀ **Fig. 8A and B.** Simulation of position and position-vestibular cell responses. **A** Change in input firing rate as a function of time for all the "push" or odd-numbered neurons. The "pull" neurons received a mirror image of this input which is omitted for reasons of graphical clarity. Every cell received the pursuit eye-velocity command which is +20 deg/s for 1 s, then −20 deg/s for 1 s. Vestibular afferents converge with the pursuit afferents for the central 16 neurons (of which the 8 odd-numbered ones are shown). The vestibular signal is a 1 s pulse for a 20 deg/s, constant-velocity, head rotation. **B** Response of the "push" or odd-numbered excitatory and inhibitory cells for the input illustrated in **A**. The central 8 records for each cell type simulate position-vestibular cells as described by Eq. (9c), and the remaining cells simulate position cell responses described by Eq. (9b)

combination of the eye-velocity signal $r_p\dot{E}_p(t)$ and $KE(t)$ as required by Eq. (9b) and (9c). During the VOR in the dark, on the other hand, neurons 8 through 23 (the central 8 odd are shown in Fig. 8b) carry the vestibular velocity signal $-r_v\dot{H}(t)$ in addition to $KE(t)$ whereas the remaining outputs modulate only by $KE(t)$. Therefore neurons 8 through 23 simulate PV cell responses, and the remaining neurons simulate P cell responses.

The parameters chosen in the Appendix are such that Eq. (9b) and (9c) are obeyed exactly for the excitatory cells. Both excitatory, P and PV cells carry the signal $1.1E(t)$ and $0.4\dot{E}_p(t)$ in Fig. 8b, and the PV cells carry $-1.0\dot{H}(t)$ as well. As explained in the Appendix, when all cells behave identically within the excitatory group and within the inhibitory group of cells (an artificial situation retained here only for simplicity), then both cell groups cannot carry the same ratio of eye-position to eye-velocity signal. The value of K was retained at 1.1 for the inhibitory group, but the velocity sensitivities had to be changed for this group. The values of r_p and r_v were 0.74 and 1.86, respectively (see Table A.3). However, if the cells within each group are not constrained, for reasons of simplicity, to be identical, then *on average* both the excitatory and inhibitory cells could have the same eye-position and eye-velocity sensitivity. Note that as predicted by the shapes of the surfaces in Fig. 7, the eye-position signal appears everywhere in the network even though the vestibular velocity input arrived on only half of its cells.

5 Discussion

We previously proposed a lateral-inhibitory network as a model for the neural integrator of the oculomotor system that circumvented the problems of robustness and the presence of background firing rates. These two problems were so basic that lesser issues were not addressed. However, there were two unrealistic aspects of the behavior of the cells in that model: they were all identical and they carried the eye-position signal but not a velocity signal contrary to the behavior of neurons in the monkey brain stem believed to be part of the integrator. The present analysis is aimed at demonstrating that the nature of the model is not incompatible with the variability seen in brain-stem neurons.

We have shown that the neurons may have a broad distribution of background firing rates. The variability of the background rates of the vestibular afferents themselves were modelled as the source of this inhomogeneity and the network simply passes this variation on in its output. It is not meant to imply that the background rates of the neurons of the integrator are supplied entirely by vestibular afferents. Observations of such neurons during sleep suggests that other sources exist. Local inhomogeneities in the intraneuronal connections, $w(k)$, can also create variations in background rates intrinsic to the network itself. Our main point was only to show that the network can tolerate such variations without losing any of its important properties. Nevertheless, since the vestibular input is a major one and has a large variability in its background rates, it is probably a major contributor. To accomodate it we discovered that it is important that the network not amplify signals with spatial frequencies other than the highest and that this came about if the arborization of the afferents had approximately the same degree of spatial spread as the collateralization of the intranetwork projections. This same modification also helps to distribute the integrated or eye-position signal to all the cells of the network even if the eye-velocity signal projects to only a local region of the network.

The largest change in the model was necessitated by the requirement that the neurons carry the eye-velocity signal. The single-layer model is intrinsically too simple to provide this capacity. Obviously, one can create cells that carry both the eye-position and eye-velocity signals by simply adding them together as in Fig. 5. The real problem is that cells that carry only the former are apparently quite rare so that the appearance of both signals must be a built-in feature of all cells in the network. A double-layer model seemed the least complicated extension of the basic idea. The inhibitory layer is still necessary to prevent the background firing rate from being integrated (lateral excitation alone does not work in this regard) while the excitatory layer adds enough dynamic complexity to enable the eye-velocity signal to be present in the outputs of both layers. It is also demonstrated that the afferents must project to *both* layers (i.e., inhibitory and excitatory cells) in order for this to happen. Also, if the intra-layer projections ($w_{ee}(k)$ and $w_{ii}(k)$) were omitted in an attempt to simplify the model, then either the excitatory or the inhibitory cells could carry the eye-position and eye-velocity signals, but the other layer would inappropriately modulate its firing rate for eye-position and eye-velocity components in opposite directions.

One of the most important demonstrations, from the standpoint of realism, is that while all cells in the network carry the eye-position signal, they may carry the eye-velocity signals with different strengths depending on the type of eye movement as shown in Fig. 8. This comes about by proposing that the velocity commands for different types of eye-movements enter the network in some regions but not others. This idea was suggested by Tomlinson and Robinson (1984) to

explain the seemingly pointless profusion of signals seen in the vestibular nucleus. The present study shows that their hypothesis is at least feasible.

An additional benefit of the double-layer model is its excitatory cells. The output of the integrator must be capable of driving motoneurons in push–pull. This requires exciting some while inhibiting others. The inhibitory cells in the single-layer model could only increase the rate of a motoneuron by disinhibition and this would require some method of offsetting its inhibitory background rate. The inclusion of both excitatory and inhibitory cells seems much more physiological. In this study subgroups of neurons in the integrator all had the same eye-position sensitivity, K, or eye-velocity sensitivity, r. We believe, however, that it would not be difficult to introduce variability in these parameters from cell to cell. For example, differences in the profiles of individual afferent arborizations to the network could cause the eye-position and eye-velocity sensitivities of each neuron to be distributed over a range of values. Figure 8 demonstrates an extreme example wherein half of the cells have no vestibular, eye-velocity sensitivity and the remaining cells do. As detailed in the Appendix, it is impossible to constrain both K_i to equal K_e and r_e to equal r_i simultaneously if each afferent profile is identical. Consequently when we used homogeneous pursuit or vestibular afferent profiles in the simulation of Fig. 8, K_e could equal K_i, but the eye-velocity sensitivity of the inhibitory neurons had to be made 1.86 times that of the excitatory ones. If we had used nonuniform profiles for one type of afferent, then it would be possible to have r_e greater than r_i for some neurons in each layer and r_e less than r_i for others so that, on average, the inhibitory and excitatory cells would have the same eye-velocity sensitivity. Since physiological evidence is not available to support or refute the proposition that on average r_e equals r_i and K_e equals K_i, we did not add the complexity of using afferent profiles that varied from one fiber to the next, but we feel that this would be one of several ways to introduce variability in cell parameters within the network.

It is also important to recognize that the type and strength of an eye-movement related response of an individual neuron in the model is a virtue of the nature of the afferent projections to the network. There is nothing intrinsically "vestibular" or "pursuit-like" for different regions of the network that was used to generate the responses in Fig. 8. The integrator pool is homogeneous and the response of an individual cell will vary with the strength and type of afferents projecting to itself and to close neighbors. In this way there could be a continuous spectrum of eye-position and eye-velocity sensitivities for individual neurons in the network. On the other hand, the poles of the network, one of which determines the degree of leakiness of the integrated signal, are dependent on the intranetwork connections alone. Consequently, if the network is at least approximately homogeneous, then the integrator time constants will be approximately equal for the eye-position component of every cell in the network.

One shortcoming of the present model concerns saccades. The velocity command for a saccade is a brief, intense, excitatory or inhibitory burst of activity. Because the integrator neurons in our latest model now encode saccadic, eye-velocity information many of them will be driven to firing rates below zero during every large saccade in one or the other direction. A nonlinearity must be introduced to simulate the pause in firing rate observed in many brain-stem neurons during large saccades. This may interfere with the ability of the network to integrate the signal correctly. The effects of this cut-off nonlinearity on the overall response of the network remain to be addressed.

For purposes of computational economy, we did not demonstrate all of the investigated features for the double-layer model. The properties by which the single-layer model coped with variations in afferent background rate were incorporated into the double-layer model and it was not felt necessary to demonstrate the solution again by specific simulation. The same is true for robustness. The fact that integration occurs through a global aspect of the network makes it independent of random, spatial alterations in its connectivity and relatively tolerant of lesions that destroy part of the network (Cannon et al. 1983). These properties are retained in the double-layer model and again it was felt unnecessary to reinvestigate the results of lesions. It would, however, be of future interest to see the effects of lesions involving only the excitatory or inhibitory layer.

This study did not explore the range of possibilities available from the double-layer model. It would be interesting for example to explore the effects on robustness of altering its six spatial distributions in various ways. Such a study could be very demanding in view of the number of possibilities. Our approach was more prosaic. We wanted to show, simply by example, that the rich variety of behavior seen on the neurons in the region of the neural integrator could be mimicked by our model.

6 Appendix

The parameter values that specify the six synaptic weighting profiles of the double-layer network were derived from the constraints implied by the Bode plot of Fig. 5, the requirement that the gain of the background signal be approximately 1.0, the requirement that for low, temporal frequencies, the gain of the

transfer function remain small for P less that π, and physiological considerations such as Dale's law and the realistic range of values that the intensity of synaptic interactions may assume. One approach that has proven, by experience, to be of great simplifying value was to first satisfy all the push–pull signal constraints when P equals π. That is, initially each synaptic profile was of concern only in that the value of its Fourier transform assume a desired value when P equalled π. Later, specific shapes could be assumed for each profile so that the remaining constraints on $\left.\frac{X(P,s)}{U(P,s)}\right|_{P<\pi}$ were satisfied. For simplicity, not necessity, delta-distributions were used whenever possible in an effort to minimize the number of parameters needed to specify a given profile.

In order to achieve the transfer properties described in Fig. 5, the transfer functions of (8a) and (8b) must fulfill the following constraints when P equals π.

1. $T_n(\pi)$ must equal 20 s which implies from the characteristic equation of (8a) or (8b) that at s equal to $\frac{-1}{T_n}$ or -0.05,

$$[s\tau_e+\beta(\pi)][s\tau_i+\alpha(\pi)]+W_{ie}(\pi)W_{ei}(\pi)=0, \tag{A1}$$

where

$$\alpha(\pi)=1+W_{ii}(\pi); \quad \beta(\pi)=1-W_{ee}(\pi).$$

2. The low-frequency asymptote of the Bode plot in Fig. 5, where s is essentially zero, implies:

a) For the excitatory cells

$$\frac{V_e(\pi)\alpha(\pi)-W_{ei}(\pi)V_i(\pi)}{\alpha(\pi)\beta(\pi)+W_{ie}(\pi)W_{ei}(\pi)}=\left(\frac{N}{N_{on}}\right)K_eT_n+r_e. \tag{A2.1}$$[5]

b) For the inhibitory cells

$$\frac{V_i(\pi)\beta(\pi)+W_{ie}(\pi)V_e(\pi)}{\alpha(\pi)\beta(\pi)+W_{ie}(\pi)W_{ei}(\pi)}=\left(\frac{N}{N_{on}}\right)K_iT_n+r_i, \tag{A2.2}$$[5]

where K and r in Fig. 5 might have different values for the excitatory (K_e, r_e) and inhibitory (K_i, r_i) cell groups.

3. The relative gain of eye-position to eye-velocity signal (i.e., zero location) is found by setting the numerators in Eqs. (8a) and (8b) to zero when s equals minus the value $(K/r)+(1/T_n)$ shown in Fig. 5, with suitable subscripts for the excitatory and inhibitory groups.

a) For excitatory cells

$$\frac{1}{\tau_i}\left[\alpha(\pi)-\frac{W_{ei}(\pi)V_i(\pi)}{V_e(\pi)}\right]=\frac{K_e}{r_e}\left(\frac{N}{N_{on}}\right)+\frac{1}{T_n}. \tag{A3.1}$$[5]

b) For inhibitory cells

$$\frac{1}{\tau_e}\left[\beta(\pi)+\frac{W_{ie}(\pi)V_e(\pi)}{V_i(\pi)}\right]=\frac{K_i}{r_i}\left(\frac{N}{N_{on}}\right)+\frac{1}{T_n}. \tag{A3.2}$$[5]

With six unknowns and five equations there is no unique solution. Rather than belabor our "trial and error" method of determining suitable parameter values from Eqs. (A1) through (A3.2), we will simply state some observations from our experiences.

(1) If attempts are made to constrain K_e to equal K_i and r_e to equal r_i, then the second root of the characteristic equation (i.e., other than the one at $-1/T_n$) effectively cancels the desired zero at $-\left(\frac{K}{r}+\frac{1}{T_n}\right)$.

(2) If $W_{ei}(\pi)$ is arbitrarily chosen to equal 1.0, then K_i is approximately $-\beta(\pi)K_e$. We chose $\beta(\pi)$ to be -1.0 so that both the excitatory and the inhibitory cells would modulate their firing rates by equal amounts in response to the eye-position signal; that is, so that K_i equalled K_e.

(3) The parameter $\alpha(\pi)$ simultaneously determines the ratio of r_i to r_e and, with $\beta(\pi)$ predetermined, the second root of the characteristic equation. As $\alpha(\pi)$ is varied so that $\frac{r_i}{r_e}$ approaches 1.0 from values greater than 1.0, the second root of the characteristic equation, as mentioned in observation (1), approaches the value of the zero, $-\left(\frac{K}{r}+\frac{1}{T_n}\right)$, and effectively cancels it. To prevent this, we compromised with the value of $\alpha(\pi)$ of 3.0 which implies that $\frac{r_i}{r_e}$ equals 1.86, and the poles of the transfer function have values s_1 of -0.05 (T_n equal to 20 s) and s_2 of -174.95 (time constant equal to 0.0057 s).

(4) Once $\alpha(\pi)$, $\beta(\pi)$, and $W_{ei}(\pi)$ were chosen the task of determining $V_e(\pi)$, $V_i(\pi)$, and $W_{ie}(\pi)$ was trivial. Their values all appear in Tables A.1 and A.2.

At this stage the only remaining task was to select the shapes of the profiles so that the gain constraints for the background firing rates of each layer were satisfied, and so that the gain of the transfer function, $X(P,s)/U(P,s)$, was low for spatial frequencies P less than π for small values of s. For convenience, but not of necessity, we chose Gaussian profiles for $v_e(k)$ and $w_{ie}(k)$ and modelled the remaining profiles as limiting cases for infinitesimally narrow Gaussian profiles, i.e., delta-distributions ($\delta(k)$). To achieve these features the spatial spread of the afferent profile, $v_e(k)$, was made greater than that of the intra-network projections, $w_{ie}(k)$. The assumed form of the profile for each type of

Table A.1. Parameter values for synaptic weighting profiles of projections intrinsic to the network

$A_{ii}=2.0$	$A_{ee}=2.0$
$A_{ei}=1.0$	
$A_{ie}=7.29085$	$\sigma_{ie}=0.2$

Table A.2. Parameter values for afferent projections used in the simulations of Figs. 7 and 8[a]

Afferent type	A_e	σ_e	$V_e(\pi)$	A_i	$\frac{N}{N_{on}}$
Pursuit velocity	0.72352	0.31195	0.350	1.04216	1.0
Vestibular velocity	2.06540	0.21020	0.875	2.60925	2.0

[a] P cells receive direct projections from pursuit velocity afferents only. PV cells receive direct projections from both pursuit and head velocity afferents

5 Note that the gain factor, K, has been scaled by $\frac{N}{N_{on}}$ as discussed in connection with Figs. 3 and 4

Table A.3. Properties of the double-layer network in terms of Fig. 5 for excitatory and inhibitory cells

Afferent type	K_e	K_i	r_e	r_i	T_n
Pursuit velocity	1.1	1.1	0.40	0.74	20
Vestibular velocity	1.1	1.1	1.0	1.86	20

projection is written below and the parameter values for the intra-network and afferent profiles are listed in Tables A.1 and A.2, respectively. Notice that the profiles intrinsic to the network assumed only one set of values while the weighting of the afferent projections extrinsic to the network are different for vestibular versus pursuit inputs. Table A.3 summarizes the overall network behavior in the context of Fig. 5

$$v_e(k) = A_e e^{-\frac{1}{2}(k/\sigma_e)^2}, \quad v_i(k) = A_i \delta(k),$$

$$w_{ee}(k) = A_{ee}\delta(k), \quad w_{ii}(k) = A_{ii}\delta(k),$$

$$w_{ei}(k) = A_{ei}\delta(k), \quad w_{ie}(k) = A_{ie} e^{-\frac{1}{2}(k/\sigma_{ie})^2},$$

whence

$$V_e(P) = A_e \sigma_e \sqrt{2\pi} e^{-\frac{1}{2}(P\sigma_e)^2}, \quad V_i(P) = A_i,$$

$$W_{ee}(P) = A_{ee}, \quad W_{ii}(P) = A_{ii},$$

$$W_{ei}(P) = A_{ei}, \quad W_{ie}(P) = A_{ei}\sigma_{ei}\sqrt{2\pi} e^{-\frac{1}{2}(P\sigma_{ie})^2}.$$

Acknowledgements. Computer graphics facilities were provided by the Johns Hopkins University Engineering Computing Facility. S.C. Cannon was supported by grants GM07309 from the General Medical Institute and EY07047 from the National Eye Institute of the National Institutes of Health (NIH), U.S. Public Health Service. D.A. Robinson received support from grant EY00598 from the National Eye Institute, NIH.

References

Becker W, Klein H (1973) Accuracy of saccadic eye movements and maintenance of eccentric eye positions in the dark. Vision Res 13:1021–1034

Cannon SC, Robinson DA (1985) Neural integrator failure from brain-stem lesions in monkey. Suppl Invest Ophthalmol Vis Sci 26, 3:47

Cannon SC, Robinson DA, Shamma S (1983) A proposed neural network for the integrator of the oculomotor system. Biol Cybern 49:127–136

Cheron G, Godaux E, Laune JM, van Derkelen B (1985) Disabling of the oculomotor neural integrator by lesions in the region of the prepositus and vestibular nuclear complex. J Physiol (Lond) (in press)

Keller EL (1974) Participation of medial pontine reticular formation in eye movement generation in monkey. J Neurophysiol 37:316–322

Papoulis A (1962) The Fourier integral and its applications. McGraw-Hill, New York, pp 42–46

Robinson DA (1975) Oculomotor control signals. In: Bach-y-Rita P, Lennerstrand G (eds) Basic mechanisms of ocular motility and their clinical implications. Pergamon Press, Oxford (Wenner-Gren Cent Int Symp Ser) pp 337–374

Robinson DA (1981) The use of control systems analysis in the neurophysiology of eye movements. Annu Rev Neurosci 4:463–503

Tomlinson RD, Robinson DA (1984) Signals in vestibular nucleus mediating vertical eye movements in the monkey. J Neurophysiol 51:1121–1136

Received: July 4, 1985

Stephen C. Cannon
Room 355 Woods Research Building
The Wilmer Institute
The Johns Hopkins Hospital
601 North Broadway
Baltimore
MD 21205
USA